Chemical Science

ROYAL SOCIETY OF CHEMISTRY

EDGE ARTICLE

View Article Online
View Journal

Cite this: DOI: 10.1039/d6sc03190k

All publication charges for this article have been paid for by the Royal Society of Chemistry

Skeletal rearrangement of [4]helicenes under acidic conditions: dynamic chirality and improved properties by subsequent peripheral editing

Arthur Gaucherand,[a] Romain Duwald,[a] Christelle Herse,[a] Céline Besnard,[b] Gennaro Pescitelli[c] and Jérôme Lacour*[a]

Cationic diaza[4]helicenes are attractive fluorescent scaffolds, yet access to unsymmetrical substitution patterns remains limited. Here, we report that chiral 1,13-dimethoxyquinacridinium (DMQA) derivatives undergo an acid-mediated skeletal rearrangement after hydride or methyl addition, enabling the sequential migration of methoxy groups and providing unprecedented 1,11- and 3,11-substituted cationic [4]helicene regioisomers. Following aerobic photooxidation, the rearranged helicenes were isolated and characterized by spectroscopy, electrochemistry, crystallography, and computation. Relative to the parent 1,13-DMQA scaffold, these core-edited systems display progressive planarization, altered redox behavior, and marked hypsochromic shifts in both absorption and emission, together with improved fluorescence efficiencies. The mono-rearranged platform further enables selective peripheral editing through S_NAr substitution and regioselective demethylation/refunctionalization, giving access to a broad family of *O*- and *N*-substituted dyes with finely tunable optical properties. Importantly, relocation of one methoxy group away from the helical groove strongly lowers the configurational barrier, affording configurationally labile helicenes with enantiomerization barriers of about 19 kcal mol^{-1}. This dynamic chirality allows asymmetric induction studies through covalently bound chiral appendages and ion pairing with an enantiopure TRISPHAT anion, leading to moderate diastereomeric enrichment and measurable ECD responses.

Received 16th April 2026
Accepted 12th May 2026

DOI: 10.1039/d6sc03190k

rsc.li/chemical-science

Introduction

Helicenes, *ortho*-fused polyaromatics, are chiral by virtue of the repulsion between the terminal rings or substituents. Their delocalized π systems generate strong interest from chemistry to biology, physics and materials science alike.[1] Helicenes – and heterohelicenes – are readily prepared by a wide variety of synthetic methods, providing large arrays of core structures.[2] Introduction of peripheral substituents, of importance to fine-tune electronic and (chiro)optical properties, is not always trivial. Often, desired functional groups must be introduced early in synthetic approaches requiring, as a consequence, the repetition of multistep sequences for each targeted product.[2i–p] In this regard, late-stage functionalization (LSF) is an appealing strategy in the context of helicenes. It remains unfortunately challenging in many instances. The presence of numerous C(sp^2)–H bonds disfavors simple chemo- and regioselectivity.[3] Sustained efforts toward novel methods of peripheral editing are investigated.[3k–m]

One class of derivatives presenting a remarkable LSF propensity is that of cationic diaza[4]helicenes **1** (Fig. 1A). These configurationally stable 1,13-dimethoxyquinacridinium derivatives ($\Delta G^{\ddagger}_{racem}$> 40 kcal mol^{-1}) are readily prepared on a multigram scale (>40 g), in two steps from dimethylresorcinol.[4] These compounds **1** present a remarkable cationic stability (pK_{R+} 19)[4b,c] and, somewhat surprisingly, a strong nucleophilic character that can be harnessed for regioselective electrophilic substitutions of diverse auxochromic functional groups, at positions *ortho*/*para* to the bridging *N*-atoms in particular (Fig. 1A).[5] Furthermore, LSF is amenable *via* metal catalysis by either metal carbene insertions or direct triple C–H borylations.[6] In this latter case, least hindered positions are favored under Ir-catalysis.[7] After C–Bpin cleavage and exchange, three electron-donating groups (EDGs) or electron-withdrawing groups (EWGs) can be introduced *para* to the formal positive charge, providing a maximal influence of these substituents. At this stage, it was clear that the introduction of a single *para*-substituent would be highly desirable, to even more precisely tune electronic and optical properties of such dyes and fluorophores. It was then debatable whether it could be achieved more

[a]*Department of Organic Chemistry, University of Geneva, Quai Ernest Ansermet 30, CH-1211, Geneva 4, Switzerland. E-mail: Jerome.Lacour@unige.ch*

[b]*Laboratory of crystallography, University of Geneva, Quai Ernest Ansermet 24, CH-1211, Geneva 4, Switzerland*

[c]*Department of Chemistry and Industrial Chemistry, University of Pisa, Via Moruzzi 13, 56124 Pisa, Italy*

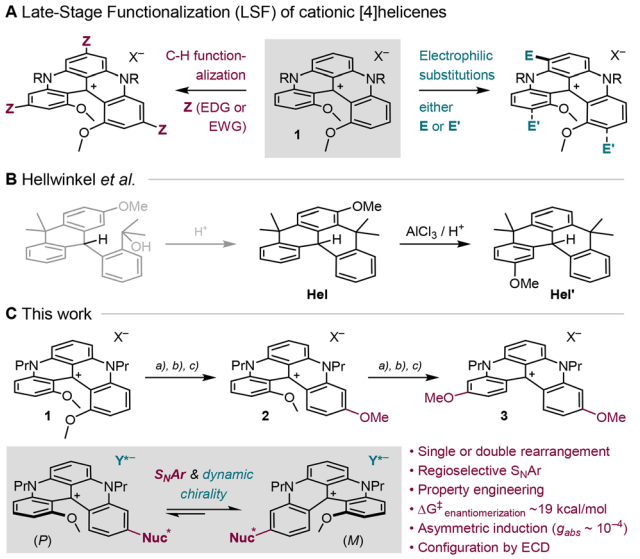

Fig. 1 (A) Functionalization of cationic [4]helicene **1** (1,13-DMQA). (B) Acid-mediated rearrangement of **HeI** into **HeI′**. (C) Access to novel 1,11-DMQA **2** and 3,11-DMQA **3**. (a) $NaBH_4$ or MeLi; (b) $MeSO_3H$; (c) photooxidation in air. **Nuc*** = achiral or stereodefinite OR, NHR, NR_2. **Y*** $^-$ = BF_4^- or TRISPHAT.

efficiently through a skeletal rearrangement rather than a *de novo* substitution.

In fact, helicenes can rearrange under rather forceful conditions (thermal, photochemical, Brønsted/Lewis acids, oxidative, *etc.*) to lead to products of intramolecular cyclization,[8] ring contraction or ring expansion,[8a,b,9] but also to the repositioning of substituents on the helical framework forming original regioisomers of the starting materials. Of particular interest to this study is the observation by Hellwinkel *et al.* that reduced all-carbon [4]helicene **HeI** transforms into its regioisomer **HeI′** upon acid treatment (Fig. 1B).[10] Nucleophilic addition to the carbenium center of **1** was therefore expected to yield an electron-rich intermediate prone to acid-promoted Friedel–Crafts fragmentation, allowing the sequential migration of the internal methoxy groups toward the peripheral *para* positions. Such a skeletal rearrangement would give access to regioisomeric DMQA scaffolds not available by direct functionalization, with direct consequences on photophysical properties and configurational stability.

Herein, in this context, we demonstrate that a combination of (i) nucleophilic additions ($NaBH_4$ or MeLi) to the cationic center of [4]helicene **1** and (ii) Brønsted acid activation affords the successive "migration" of the internal methoxy groups toward peripheral *para* positions (Fig. 1C). Aerobic photooxidation then affords rearranged cations **2** and **3**, presenting modified structural, electronic and optical properties. For instance, hyperchromism and hypsochromism demonstrate a stronger electron-donating efficiency of the *para* MeO substituents. Product **2** is also a substrate for further LSF. Aromatic nucleophilic substitutions (S_NAr) with diverse alcohols and amines afford products **4** and **5** while regioselective demethylation/refunctionalization of the more accessible *p*-OMe substituent generates phenol **6** and ester **7**. All subsequent optical properties are in line with the expected electron-donating (or withdrawing) influence of the modified groups. Finally, the configurational stability of derivatives **2** (*p*-OMe), **4** (*p*-OR) and **5** (*p*-NR_2) is drastically reduced with a single MeO substituent inside the helical groove ($\Delta G^{\ddagger} \sim 19 \pm 1$ kcal mol^{-1}), opening the door to asymmetric induction (dynamic chirality) studies monitored by ^{1}H-NMR and electronic circular dichroism (ECD) spectroscopy. The presence of intra- and/or intermolecular chiral auxiliaries leads to the preferred formation of diastereomeric species with moderate levels of selectivity (diastereomeric ratio, *d. r.* up to 2 : 1); the favored sense of induction being assigned by ECD, with experimental $|g_{abs}|$ values up to $9{\cdot}10^{-5}$, allied with TD-DFT investigations.

Results and discussion

Skeletal rearrangement procedures

1,13-Dimethoxyquinacridinium (1,13-DMQA) **1** was prepared as its tetrafluoroborate salt (BF_4^-) in two steps from 1,3-dimethoxybenzene (40 g scale).[4b,d,e] As mentioned, this carbenium ion is particularly stable,[4b,c] yet it is amenable to hydride addition with reagents like $NaBH_3CN$ or $NaBH_4$.[4b,11] With 4 equiv. of sodium borohydride, neutral **1-H** was obtained in high isolated yield (96%, Scheme 1). Importantly, treatment of *leuco* **1-H** under strongly acidic conditions ($MeSO_3H$, 2 equiv., pK_a −1.9)[12] led after 22 h at 80 °C to a complex crude mixture from which several compounds could be identified, including, as a major component, product **2-H**. High-resolution mass spectrometry indicated a derivative of the same molecular mass as **1-H** but the lack of C_2-symmetry in the ^{1}H NMR spectrum pattern was clearly indicative of a skeletal rearrangement. For **2-H**, only a structure with one MeO group inside the groove and one external MeO *para* to the formal center of the helical derivative was possible.[13] Minor fractions of carbocations **1** and **2** were also observed despite the controlled anaerobic atmosphere (Ar). Stronger acidic conditions (TfOH, 2 equiv., pK_a −14)[14] gave evidence for a rearrangement proceeding even further toward the migration of both MeO groups, but isolation of corresponding **3-H** was ultimately challenging. To simplify work-up and purification steps, eventually realizing that most interesting compounds are (reoxidized) carbenium ions **2** and **3** and

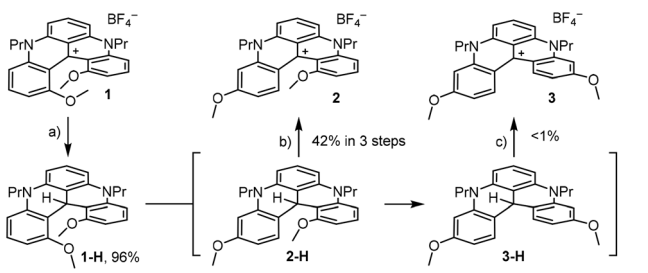

Scheme 1 (a) $NaBH_4$ (4.0 equiv.), MeOH, rt, 5 min. (b) $MeSO_3H$ (2.0 equiv.), DCE, 80 °C, dark, 16 h; air, white light, $NaBF_4$ (aq.):DCM, 25 °C, 2 h. (c) TfOH (2.0 equiv.), DCE, 80 °C, dark, 20 h; air, white light, $NaBF_4$ (aq.):DCM, 25 °C, 2 h.

not their hydride precursors, care was taken to treat crude reaction mixtures directly under air and white-light irradiation (2 h) in the presence of aqueous $NaBF_4$ (excess). While carbocation **2** could be isolated in 42% yield over the three combined steps, doubly rearranged **3** was isolated with ~1% yield only.

To improve the synthesis of **3**, and in light of a mechanism involving most probably reversible Friedel–Crafts reactions (*vide infra*), the rearrangement was attempted with **1-Me** (Scheme 2), derived from cation **1** by treatment with methyllithium (excess). With this activated adduct,[15] the double skeletal rearrangement proceeded toward **3-Me** with "milder" methanesulfonic acid. Of interest, subsequent oxidation (air, white light) afforded **3** with a better isolated yield (46%) after a C–Me bond cleavage.[16]

Skeletal rearrangement – mechanistic rationale

To explain the rearrangement of **1-R** (R=H, Me) into corresponding **2-R** and then **3-R**, a mechanism building on reversible Friedel–Crafts reactions can be considered (Scheme 3).[17] In fact, thanks to the electron-rich nature of each aromatic group after hydride addition (R=H) or alkylation (R = Me) of the central position, protonation of derivatives **1-R** occurs readily under strongly acidic conditions to lead to stabilized Wheland intermediates of type **Ia** (Scheme 3, left column). Then, helped by the release of strain generated by the proximity of the MeO groups, *retro*-Friedel–Crafts reactions occur,[18] yielding ring-opened intermediates **IIa** by fragmentation (C–C bond cleavage). Free rotation around the C–N bond of the detached aromatic ring (**IIa** → **IIIa**) then positions the less hindered and more nucleophilic side of the moiety, favoring the reformation of a sterically more favored arenium intermediate (**IIIa** → **IVa**). Final proton loss yields **2-R** that can be observed spectroscopically.

The next rearrangement, from **2-R** to **3-R**, follows homologous steps onto the remaining *ortho*-OMe substituted terminal ring (Scheme 3, right column). The presence of the central methyl group in **Ib**, **IIb**, **IIIb** and **IVb** transforms these cations from secondary to tertiary intermediates, rendering the species more electrofugal and hence better intramolecular leaving groups. This is reflected in the better yield of **3** starting from **1-Me** over **1-H** under the same conditions ($MeSO_3H$, 80 °C).

Structural crystallographic analysis

With rearranged dimethoxyquinacridinium **2** and **3** in hand, attention was immediately given to their geometry. Under slow-evaporation conditions, single crystals were isolated, and X-ray structural analyses were performed (Fig. 2, CCDC 2542615 and 2542616) and compared with those of classical **1** (CCDC 2319499

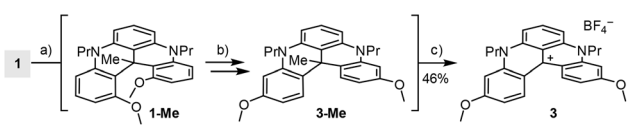

Scheme 2 (a) MeLi (5.0 equiv.), THF, −78 °C, 16 h. (b) $MeSO_3H$ (2.0 equiv.), DCE, 80 °C, dark, 18 h. (c) Air, white light, $NaBF_4$ (aq.):DCM, 25 °C, 2 h.

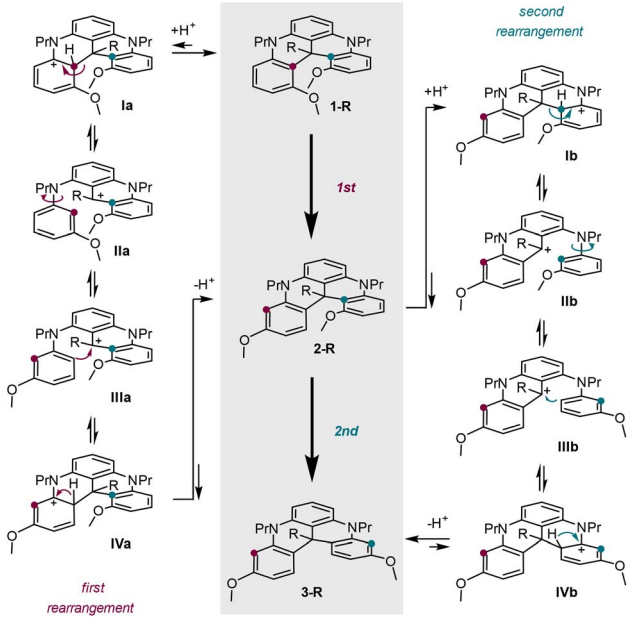

Scheme 3 Acid-mediated transformation of **1-R** into **2-R** and **3-R** (central column, R = H or Me). Mechanistic rationale for first (left) and second (right) skeletal rearrangements.

and 2319500).[19] To quantify the helicity, three parameters were selected (Fig. 2 and Table S3): (i) the interplanar angle ψ between the planes of the terminal rings, which reflects the compactness of the structure, (ii) the mean torsion angle between four consecutive atoms inside the groove φ, and (iii) the pitch d that measures the distance between the carbons at the cove positions. As it could be expected, the helical deformation decreases from **1** to **2** and then to **3**, with φ values lessening from 27.1° (**1**) to 23.8° (**2**) and 18.9° (**3**). The skeletal helicity remains nevertheless noticeable despite a gradual loss of steric hindrance inside the cove brought by the lack of MeO group(s). A certain planarization occurs with ψ changing from 40.5° → 38.6° → 29.3° for **1** → **2** → **3**; the effect of this angle reduction will later be monitored in terms of electronic and optical properties. Consequences of the structural changes will also be investigated in terms of configurational stability (*vide infra*).

Electrochemical and photophysical properties

Compounds **2** and **3** were studied by cyclic voltammetry (CV) in acetonitrile under an inert atmosphere (Ar) and the results were

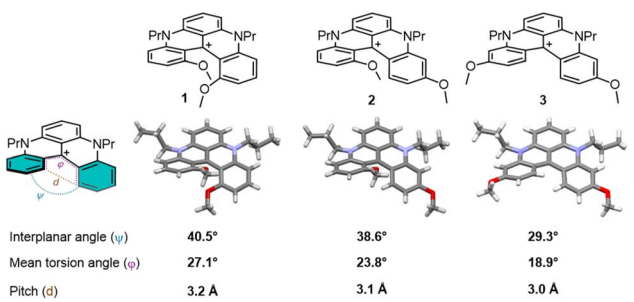

Fig. 2 Selected structural features of DMQA **1**, **2** and **3**.

compared with those of **1** (Table 1 and Fig. 3). In effect, precursor **1** presents reversible first reduction at −1.23 V (*vs.* Fc^+/Fc, ΔE_p = 75 mV and $i_b/i_f \sim 1$), a second irreversible reduction at −2.11 V (not shown), and a quasi-reversible oxidation at +0.88 V.[4b,20] Peripheral editing into **2** and **3** gradually influenced the first reductions that became more difficult ($E_{1/2}^{red}$ −1.28 V and −1.35 V for **2** and **3**, respectively), while oxidation potentials remained constant ($E_{1/2}^{ox}$ +0.87 V).

The presence of an irreversible second reduction is still observed for **2** and **3**. Overall, compared to **1**, oxidation and reduction processes are poorly reversible with low ratios between current intensity backward and forward ($0.5 < i_b/i_f < 0.7$).

Then, absorption and emission spectra of **2** and **3** were recorded in acetonitrile, and fluorescence quantum yields/lifetimes were determined (Fig. 4 and Table 2). 1,13-DMQA **1** displays a relatively broad absorption band with a maximum at 616 nm and an emission maximum at 666 nm, with a fluorescence quantum yield (Φ_f) of 14% and a lifetime (τ) of 5.6 ns.[6b,21] Upon rearrangement, tetrafluoroborate salts **2** and **3** present hypsochromic shifts of both absorption and emission (λ_{max} 616 → 587 → 562 nm and λ_{em} 666 → 642 → 622 nm for **1** → **2** → **3**), which indicates a good correlation between optical and electrochemical energy gaps (Tables 1 and 2). Consistent with the energy gap law, the general blue-shift is also followed by an increase in Φ_f and τ. The experimental optical energy gap, absorption maximum and reduction potential of compounds **1**–**3** correlate well with the HOMO–LUMO gap, S_0–S_1 transition energy and LUMO energy, respectively, calculated with (TD-) DFT (Fig. S100). Overall, the hypsochromic shift is explained by a stronger electron-donating character of methoxy groups in *para* to the formal positive charge, allied with the gradual planarization of the helical skeleton, assuring a stronger influence of the *p*-OMe substituents and a progressive rise in LUMO energy (Fig. S101).

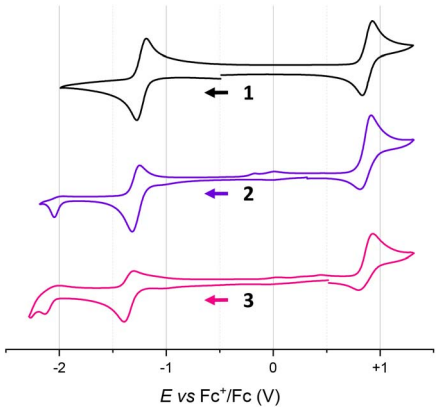

Fig. 3 Cyclic voltammetry curves of **1** (black), **2** (purple), and **3** (pink) recorded at the Pt electrode (Ø = 3 mm and ν = 0.1 V s^{-1} for **1** and ν = 0.02 V s^{-1} for **2** and **3**) with a concentration of 5 × 10^{-4} M in dry acetonitrile under an inert atmosphere using [^{n}Bu$_4$N][PF$_6$] 10^{-1} M as supporting electrolyte. The arrow indicates the direction of the scan (negative potential first).

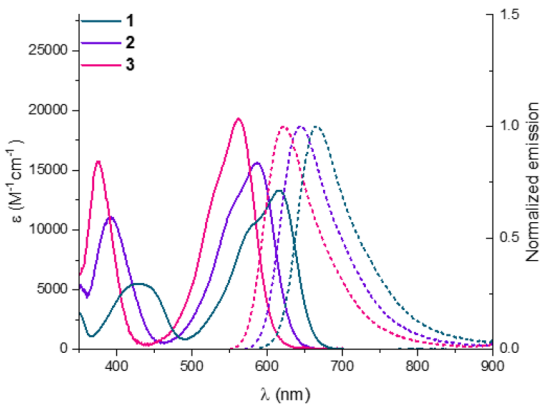

Fig. 4 Absorption and normalized emission spectra of **1** (green), **2** (purple), and **3** (pink) in air-equilibrated MeCN at 20 °C with concentrations of 1 × 10^{-5} to 3 × 10^{-5} M.

Subsequent reactivity and induced properties

Then, with compound **2** readily accessible, late-stage functionalizations were tackled to expand possible derivatives of study. As expected from previous investigations, and that of Laursen *et al.* in particular,[4a,22] regioselective substitutions of *p*-OMe substituents occurred in the presence of various alcohols and amines (Fig. 5). Nucleophilic aromatic substitutions (S_NAr) were prone to occur on the MeO group at position 11, by virtue of its less-hindered position, *para* to the formal positive charge. The other MeO group, inside the helical cove, was clearly less reactive. Faster kinetics and improved yields were obtained when nucleophiles were used directly as solvents. With ethanol and isopropanol as media, ethers **4a** and **4b** were generated in the presence of K_2CO_3 and at relatively high temperatures (reflux, 78 or 82 °C). In both instances, partial reduction of the carbocations occurred during reactions due to the hydride-donating ability of these solvents, with a predilection for isopropanol.[23,24]

An extra step of photooxidation (air, white-light irradiation, 25 °C) was then required to convert reduced neutral adducts into desired cations **4a** (87%) and **4b** (62%).[25] With *tert*-butanol, formation of **4c** could not be achieved due to the steric hindrance of the tertiary alcohol precluding the S_NAr reactivity.

Table 1 Electrochemical data of DMQA regioisomers in acetonitrile[a]

Molecule	$E_{1/2}^{red,1}$ (ΔE_p)	i_b/i_f	$E_{1/2}^{ox}$ (ΔE_p)	i_b/i_f	Electrochemical energy gap (eV)
1[b]	−1.23 (75)	0.96	+0.88 (90)	0.83	1.98
2[c]	−1.28 (68)	0.67	+0.87 (99)	0.59	1.99
3[c]	−1.35 (90)	0.51	+0.87 (126)	0.50	2.08

[a] $E_{1/2}$ (V, *vs.* Fc^+/Fc) and peak-to-peak separations (ΔE_p in mV), and the ratio between current intensity back (i_b) and forward (i_f) for the redox processes exhibited at the Pt electrode by compounds **1**, **2**, and **3** (5 × 10^{-4} M) in dry acetonitrile with [^{n}Bu$_4$N][PF$_6$] 10^{-1} M as supporting electrolyte. [b] Measured with ν = 0.1 V s^{-1}. [c] Measured with ν = 0.02 V s^{-1}.

Table 2 Photophysical data of rearranged DMQA derivatives in acetonitrile

Molecules[a]	λ_{max} (nm)	ε (M^{-1} cm^{-1})	λ_{em} (nm)	Stokes shift (cm^{-1})	Φ_f[b] (%)	τ[e] (ns)	k_r[f] (10^6 s^{-1})	k_{nr}[g] (10^6 s^{-1})	Optical energy gap E_{00} (eV)
1	616	13 321	666	1219	14[c]	5.6	25	154	1.94
2	587	15 634	642	1460	24[d]	7.8	31	97	2.02
3	562	19 360	622	1717	43[d]	10.7	40	53	2.10

[a] Concentrations are 1×10^{-5} to 3×10^{-5} M. [b] Φ_f estimated error = ±10%. [c] Oxazine 170 perchlorate (Φ = 58% in EtOH). [d] Cresyl violet perchlorate (Φ = 58% in EtOH). [e] λ_{exc} = 400 nm. [f] $k_r = \Phi_f/\tau$. [g] $k_{nr} = (1 - \Phi_f)/\tau$.

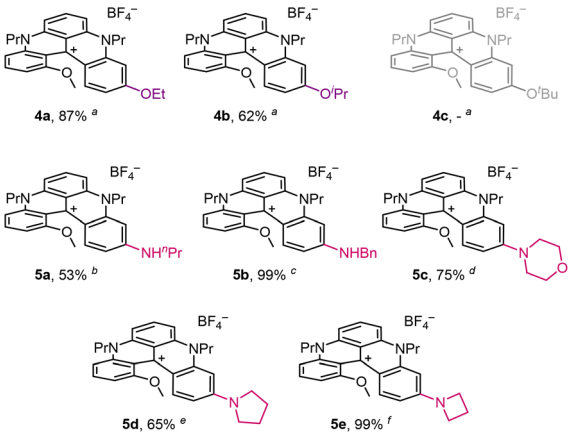

Fig. 5 Synthesis of ethers **4** and anilines **5** starting from **2** as a substrate. [a](i) K_2CO_3, (2.0 equiv.) ROH, reflux, 24 h; (ii) air, white light, $NaBF_4$ (aq.):DCM, 25 °C, 2 h. [b] $^nPrNH_2$, 20 °C, 96 h. [c] $BnNH_2$, 40 °C, 48 h. [d] Morpholine, 80 °C, 5 h. [e] Pyrrolidine, 80 °C, 19 h. [f] Azetidine, 20 °C, 72 h.

With more nucleophilic primary amines as solvent, products **5a** (53%) and **5b** (99%) containing *n*-propyl and benzylamino residues were prepared at 20 or 40 °C, respectively. Higher temperatures (80 °C) were nevertheless necessary for the syntheses of morpholinyl **5c** and pyrrolidinyl **5d** derivatives in 75% and 65% yields, respectively. For the introduction of an azetidine moiety, lower temperature (20 °C) and longer reaction times were selected to yield corresponding derivative **5e** in virtually quantitative yield (99%).

Alternatively, by treatment of **2** with BBr_3, regioselective demethylation of the more accessible *p*-OMe group gave access to phenol **6** (Scheme 4). Counterion exchange between BF_4^- and PF_6^- led to a more soluble salt in dichloromethane and an easier overall purification. With **6** in hand, alkylation reactions with isopropyl iodide and benzyl bromide afforded **4b** (46%) and **4d** (99%) in moderate and excellent yields, respectively. Finally, acetylation of **6** gave rapid access to ester **7**.

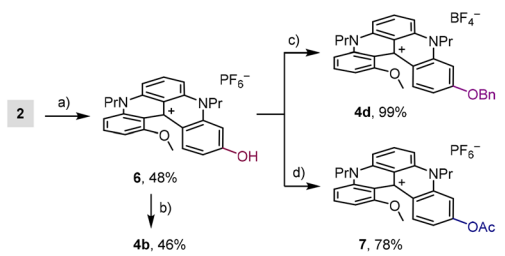

Scheme 4 (a) (i). BBr_3 (5.0 equiv.), CH_2Cl_2, 0 to 20 °C, 72 h; (ii). anion metathesis with KPF_6 (aq.). (b) Cs_2CO_3 (2.5 equiv.), ^iPrI (20 equiv.), DMF, 20 °C, 40 h. (c) (i). Cs_2CO_3 (2.5 equiv.), BnBr (20 equiv.), DMF, 20 °C, 2.5 h; (ii). anion metathesis with $NaBF_4$ (aq.). (d) Et_3N (2.0 equiv.), AcCl (3.0 equiv.), CH_2Cl_2, 20 °C, 15 min.

Photophysical properties

With compounds **4** to **7** in hand, absorption and emission spectra were recorded in acetonitrile (Table 3 and Fig. S9–S14) with selected examples presented in Fig. 6 and 7. As expected, few differences were observed between **2**, **4a** and **4d** upon the change of the ether terminal group (Me → Et → Bn, Fig. S9). With sterically more encumbered **4b** (isopropyl), a hypochromic effect (ε 11 746 M^{-1} cm^{-1}) was noticed that cannot be readily explained at this stage. For ester **7**, allied with the electron-deficient nature of the acetyl group, a bathochromic shift was noticed in both absorption and emission (λ_{max} 611 nm and λ_{em} 664 nm).[6b] As a consequence, a decrease of Φ_f (8%) and τ (1 ns) was also observed in comparison with **2** (Fig. 6A).

Regioselective substitution of the outer MeO group by amino groups afforded a global blue-shift of optical properties with (large) differences upon the moieties attached (Fig. 6B). Globally, higher values were obtained for the molar extinction coefficients (ε), Φ_f, and τ, reaching numbers up to 21 128 M^{-1} cm^{-1}, 54% and 13 ns for **5b** (NHBn). Even stronger values were expected for azetidine **5e** in view of literature precedents indicating a stronger donor character for such auxochromes.[26] In effect, values increased to 27 253 M^{-1} cm^{-1} for ε, 50% for Φ_f and 12.1 ns for τ.

Finally and not surprisingly, phenol **6** proved to be pH-sensitive.[27] It was briefly studied under acidic and basic conditions, *i.e.* in the presence of AcOH or Et_3N in acetonitrile (Fig. 7). With AcOH, phenol **6** displayed properties similar to those of **2** while, with Et_3N, large hypso- and hyperchromic shifts (λ_{max} 511 nm and ε 25 618 M^{-1} cm^{-1}) were observed along with a broadening of absorption and emission bands.

For **6**, a remarkably large Stokes shift (3569 cm^{-1}), albeit with low Φ_f and τ values (4% and 1 ns), is recorded; all data are consistent with those of a neutral quinone form under basic (deprotonated) conditions.

Configurational lability (dynamic chirality) and asymmetric induction

Finally, consistent with the X-ray structural analysis that demonstrated a largely helical skeleton for **2** (*vide supra*),

Table 3 Photophysical data of rearranged DMQA derivatives in acetonitrile

Molecules[a]	λ_{max} (nm)	ε (M^{-1} cm^{-1})	λ_{em} (nm)	Stokes shift (cm^{-1})	Φ_f[b] (%)	τ (ns)	k_r[h] (10^6 s^{-1})	k_{nr}[i] (10^6 s^{-1})	Optical energy gap E_{00} (eV)
OEt (**4a**)	586	17 389	642	1489	25[c]	8.5[e]	29	88	2.02
OiPr (**4b**)	585	11 746	643	1542	27[c]	8.4[f]	32	87	2.02
OBn (**4d**)	588	17 192	643	1455	24[c]	7.6[g]	32	100	2.02
OAc (**7**)	610	15 420	664	1306	8[c]	1.0[e]	80	920	1.95
NHnPr (**5a**)	557	20 431	614	1667	57[c]	12.7[f]	45	34	2.12
NHBn (**5b**)	562	21 128	617	1586	54[c]	13.0[e]	42	35	2.11
Morpholinyl (**5c**)	569	18 482	633	1777	38[c]	10.1[e]	38	61	2.07
Pyrrolidinyl (**5d**)	559	13 963	613	1576	46[c]	12.0[e]	38	45	2.12
Azetidinyl (**5e**)	557	27 253	620	1824	50[c]	12.1[g]	41	41	2.11
OH (**6**) + Et_3N[j]	511	25 618	625	3569	4[d]	1.0[e]	40	960	2.21
OH (**6**) + AcOH[k]	586	15 098	638	1391	29[c]	8.0[e]	36	89	2.03

[a] Concentrations are 1×10^{-5} to 3×10^{-5} M. [b] Φ_f estimated error = ±10%. [c] Cresyl violet perchlorate ($\Phi = 58\%$ in EtOH). [d] Rhodamine B ($\Phi = 70\%$ in MeOH). [e] $\lambda_{exc} = 470$ nm. [f] $\lambda_{exc} = 395$ nm. [g] $\lambda_{exc} = 400$ nm. [h] $k_r = \Phi_f/\tau$. [i] $k_{nr} = (1 - \Phi_f)/\tau$. [j] 1% of Et_3N was added to the solvent. [k] 1% of AcOH was added to the solvent.

further investigations proved the occurrence of chiral geometries for mono-rearranged products in solution and that of compounds **4** and **5** in particular. However, it became rapidly clear that such compounds lacked configurational stability. While room temperature ^{1}H-NMR analyses of **4d** (OBn) and **5b** (NHBn) supported the existence of residual stereoisomerism, since benzylic protons presented anisochronous doublet signals, heating in either $CDCl_3$ or CD_3CN of compound **4d** (Fig. S1) resulted in coalescence of these diastereotopic protons above 80 °C ($\Delta\delta$ 0.03 pm at 20 °C). Line-shape analysis of the dynamic exchange was realized for the acetonitrile solution and afforded kinetic constants at different temperatures (Table S1). Using Arrhenius and Eyring kinetic analyses (Table S2), activation energy E_a (22.8 ± 0.7 kcal mol^{-1}), pre-exponential factor A ($2.5 \times 10^{15} \pm 8 \times 10^{13}$), enthalpy of activation $\Delta H^{\ddagger}$ (22.2 ± 0.7 kcal mol^{-1}) and entropy of activation $\Delta S^{\ddagger}$ (10.0 ± 0.3 cal K^{-1} mol^{-1}) were determined. Assuming consistency between solid-state and solution geometries, compound **4d** interconverts between enantiomeric *M* (left-) and *P* (right-handed) helical conformers with a barrier of $\Delta G^{\ddagger}$ 19.2 ± 0.8 kcal mol^{-1} (80.4 kJ mol^{-1}) at 298 K. The much lowered kinetic barrier, in comparison with **1** ($\Delta G^{\ddagger}_{473}$ 41.3 kcal mol^{-1}),[4d] is the direct consequence of the reduced repulsion between the terminal ends of the helix brought by the loss of one MeO group in the groove (cove) area.

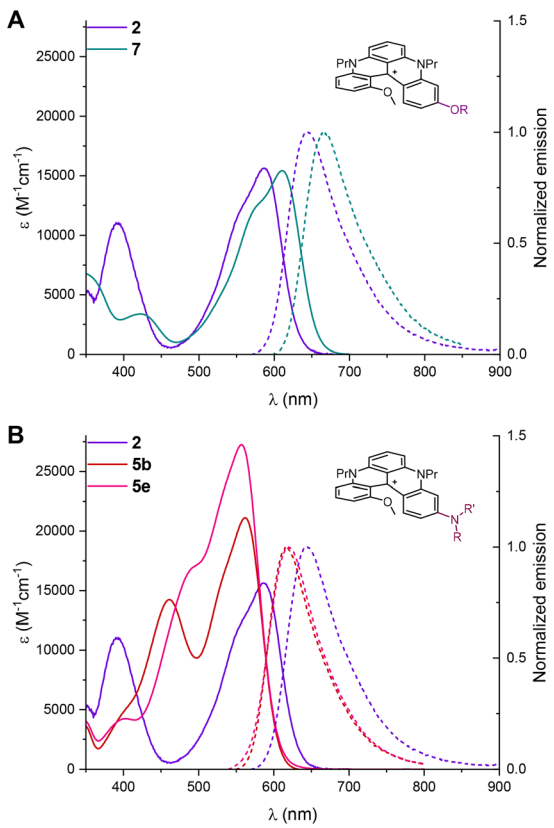

Fig. 6 Absorption and normalized emission spectra in air-equilibrated MeCN at 20 °C with concentrations of 1×10^{-5} to 3×10^{-5} M. (A) **2** (purple) and **7** (green); (B) **2** (purple), **5b** (red), and **5e** (pink).

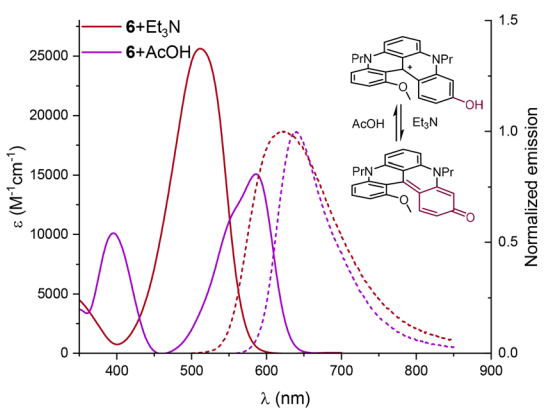

Fig. 7 Absorption and normalized emission spectra of **6** in presence of an excess of either Et_3N (red) or AcOH (purple) in air-equilibrated MeCN at 20 °C with concentrations of 1×10^{-5} to 3×10^{-5} M.

For all compounds **2** and **4–7**, enantiomerization barriers remain probably in the same range (19 ± 1 kcal mol^{-1}) and, consequently, these moieties are chiral yet configurationally labile, with half-lives in the range of seconds at 20 °C. The *M* and *P* enantiomers interconvert thus freely in solution (dynamic chirality), and the possibility of shifting the 1 : 1 equilibrium toward one preferred configuration was then debatable.[28,29] In fact, several approaches could be considered to induce diastereoselective interactions in relation to scaffolds **4** and **5**. Two such strategies were tried successively and then combined.

In a first attempt, stereodefinite exocyclic substituents were introduced to impose, ideally, intramolecular discriminating interactions onto the chiral helical geometry. Practically, (*S*)-citronellol, (*S*)– and (*R*)-1-phenylethylamine were reacted with **2** under previously detailed conditions to generate products (*S*)-**4e** (39%), (*S*)-**5f** (93%) and (*R*)-**5f** (99%), in moderate to good yields (Scheme 5). While a minimal amount of discrimination was observed in ^{1}H (and ^{13}C) NMR spectra of (*S*)-**4e** (Fig. S45), a moderately better split of the signals was afforded for the interconverting diastereomers of (*S*)– or (*R*)-**5f**. In practice (Fig. 8A), doublet signals of the methyl group (red color) adjacent to the stereogenic center were separated but the signal separation was not large enough to permit a reliable integration. The NMR split was better for the internal MeO group (green color) yet with a strong broadening for one diastereomeric structure, also limiting the precision of the stereoselectivity measurement (*d. r.*∼1.35 : 1). The asymmetric induction was confirmed by ECD analyses. Whereas 3 Cotton effects were detected above 350 nm for amino (*S*)– and (*R*)-**5f** (Fig. 8B) and presented the expected mirror image relationship (red and blue traces), no induction could be observed for (*S*)-**4e** (Fig. S2). For the enantiomers of **5f**, g_{abs} dissymmetry factor values were measured in the range of ±5 10^{-5} for the lowest energy band reflecting the small level of asymmetric induction observed in ^{1}H-NMR spectroscopy.

To determine the absolute sense of asymmetric induction, the ECD spectra of (*R*)-**5f** were calculated using time-dependent density functional theory (TD-DFT) after DFT geometry optimizations. CAM-B3LYP and B3LYP were screened as functionals for excited-state calculations as they generally provide good accuracy for helicene-type compounds;[30] in the current case, B3LYP yielded a better agreement. ECD spectra were calculated for (*M*)–(*R*)-**5f** and (*P*)–(*R*)-**5f** diastereomers and showed a quasi-mirror image relationship being dominated by the helicity of the diaza[4]helicene core (Fig. S102). (*M*)–(*R*)-**5f** had 3 positive ECD bands at above 350 nm, in accordance with the experimental spectrum of (*R*)-**5f** (Fig. 8B). Thus, (*R*)-1-phenylethylamine induces preferential (*M*)-helicity, as shown in Scheme 5. We notice that the calculated g_{abs} for the lowest-energy ECD band of **5f** is 2.4 10^{-4}, which fits well the experimental value of 5 10^{-5} considering a diastereomeric excess of 20% (0.2 × 2.4 10^{-4} = 4.8 10^{-5}) and the fact that the two diastereomers have calculated mirror-image ECD spectra. Molecular orbital (MO) analysis revealed that the 3 ECD bands all involve the same LUMO, delocalized over the whole diaza[4]helicene core, but different occupied MOs with different degrees of delocalization: the first transition (HOMO–LUMO) is localized, while the following two have a pronounced charge-transfer (CT) character (Fig. S103).

The second asymmetric induction strategy used a diastereoselective ion pairing approach with enantiopure hexacoordinated tris(tetrachlorobenzenediolato)phosphate anion **8**, namely TRISPHAT, as a chiral auxiliary. This moiety **8**, made in one step by the condensation of PCl_5 and anhydrous tetrachlorocatechol, is resolved into single Δ and Λ enantiomers (right and left-handed three-bladed propellers) with

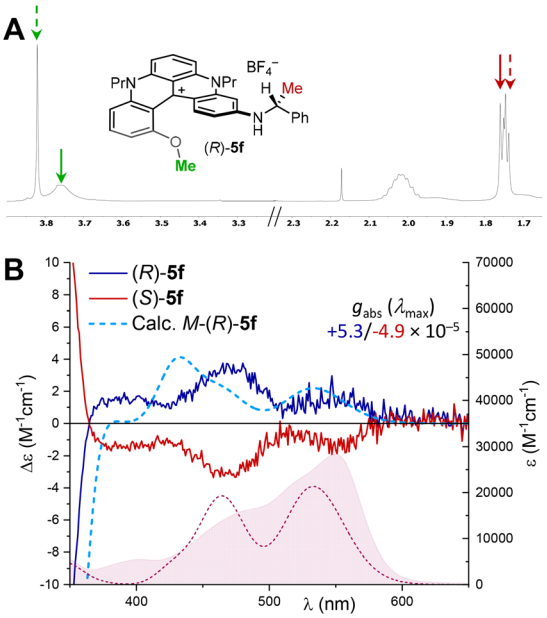

Fig. 8 (A) ^{1}H-NMR spectra in $CDCl_3$ at 298 K, 500 MHz of [(*R*)-**5f**][BF_4]; (B) ECD spectra and absorption spectra (underlying filled curve) in air-equilibrated chloroform at 20 °C of [(*S*)-**5f**][BF_4] (red) and [(*R*)-**5f**][BF_4] (blue), *c* 3–4 × 10^{-5} M. Dotted lines: calculated ECD and absorption spectra of (*M*)–(*R*)-**5f** at the B3LYP/def2-TZVP/PCM//B3LYP-D3BJ/6-31+G(d)/PCM level (IEF-PCM solvent model for $CHCl_3$), plotted as sums of Gaussians with $\sigma = 0.15$ eV, red shifted by 25 nm, and scaled by a factor of 3.5.

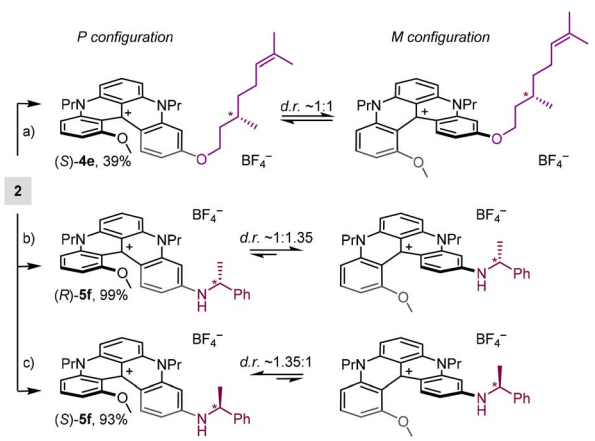

Scheme 5 (a) (i) K_2CO_3, (−)-citronellol, 80 °C, 4.5 h; (ii) $NaBF_4$ (aq.):DCM, 20 °C, air, white light. (b) (*R*)-$PhEtNH_2$, 70 °C, 4–7 days. (c) (*R*)-$PhEtNH_2$, 70 °C, 4–7 days.

cinchonidine as a resolving agent.[31] This anion is an excellent NMR chiral solvating agent, able to distinguish enantiomers among many different types of chiral cationic reagents,[32] but it is also an effective chiral auxiliary to control the configuration of labile moieties (Pfeiffer effect).[29a,c,33] In practice, ion metatheses of BF_4 to Δ- or Λ-**8** anions were realized by mixing equimolar amounts of precursor salts, *e.g.* [**5b**][BF_4] and [cinchonidinium][Δ-**8**] or [Bu_3NH][Λ-**8**] followed by rapid chromatography over silica gel (eluent CH_2Cl_2). The desired ion pairs [**5b**][Δ-**8**] and [**5b**][Λ-**8**] were isolated as the only migrating fractions (>90% yield). In ^{1}H-NMR spectra, the signals of (*M*)/(*P*)-**5b** were well distinguished in the presence of anions **8** and the MeO signals in particular (Δδ 0.12 ppm, Fig. 9A). Clear integration of the signals revealed a small induction (*d. r.* 1.25 : 1), confirmed again by ECD measurements (Fig. 9B). In view of the previous configurational assignment by ECD analysis, and since ECD is dominated by the diaza[4]helicene core, the Δ and Λ enantiomers of anion **8** provoke an equilibrium shift toward (*M*)-**5b** and (*P*)-**5b**, respectively. Finally, as can be expected, choosing a polar solvent like CD_3CN reduces the coulombic attraction within the ion pair and leads to a lack of NMR chiral solvating efficiency of the TRISPHAT anion (Fig. S93) and to an absence of diastereoselectivity in ECD spectroscopy (Fig. S3).

Care was then taken to benefit from both the intramolecular and supramolecular (ionic) asymmetric induction strategies, trying to complement the influence of the stereogenic benzylamine substituent with the stereodefinite counterion. Diastereomeric salts [(*R*)-**5f**][Δ-**8**] and [(*S*)-**5f**][Δ-**8**] were prepared as above using the corresponding TRISPHAT source and their

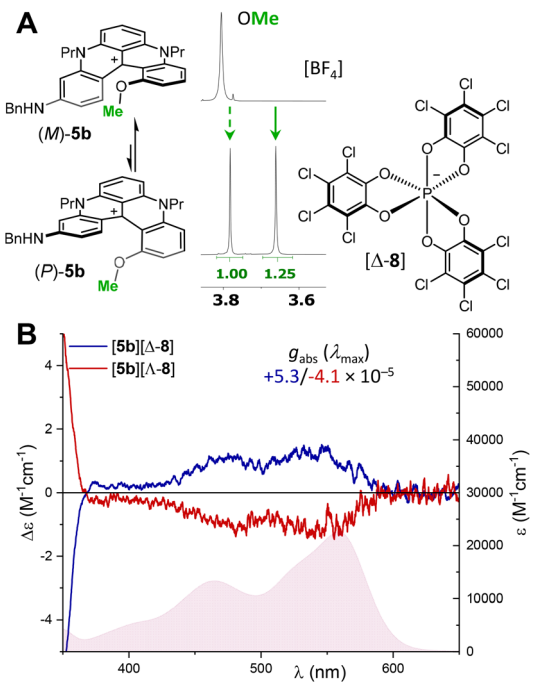

Fig. 9 (A) ^{1}H-NMR spectra ($CDCl_3$, 298 K, 500 MHz) of [**5b**][BF_4] and [**5b**][Δ-**8**] (Δ-enantiomer of TRISPHAT **8** is shown). (B) ECD spectra and absorption spectra (underlying filled curve) in air-equilibrated chloroform at 20 °C of [**5b**][Λ-**8**] (red) and [**5b**][Δ-**8**] (blue), *c* 3–4 × 10^{-5} M.

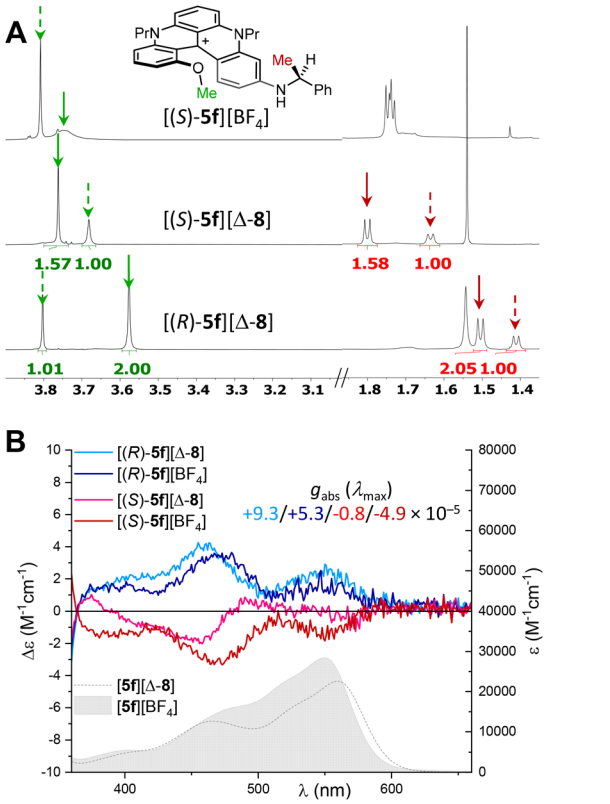

Fig. 10 (A) ^{1}H-NMR spectra ($CDCl_3$, 298 K, 500 MHz) of [(*S*)-**5f**][BF_4], [(*S*)-**5f**][Δ-**8**] and [(*R*)-**5f**][Δ-**8**] with *d. r.* 1.35 : 1, 1.6 : 1 and 2.0 : 1, respectively. (B) ECD spectra and absorption spectra (underlying filled curve, **5f** corresponding salt) in air-equilibrated chloroform at 20 °C of [(*S*)-**5f**][BF_4] (red), [(*R*)-**5f**][BF_4] (blue), [(*S*)-**5f**][Δ-**8**] (pink), and [(*R*)-**5f**][Δ-**8**] (light blue).

NMR spectra were compared with that of [**5f**][BF_4] salts in $CDCl_3$ (500 MHz, ^{1}H-NMR, Fig. 10A). Not surprisingly, salts [(*R*)-**5f**][Δ-**8**] and [(*S*)-**5f**][Δ-**8**] presented well distinguished and dissimilar signals for the interconverting diastereomers in ^{1}H-NMR, with a more pronounced nonequivalence of the MeO signals for ion pairs (*R*, Δ) over (*S*, Δ) (Δδ 0.23 *vs.* 0.08 ppm, respectively). Integration of the signals revealed small but definite differences among the diastereomeric ratios (*d. r.* 2.0 : 1 *vs.* 1.6 : 1) for the two pairs.

A difference could also be monitored in ECD spectroscopy. In fact, while ECD spectra of [(*S*)-**5f**][BF_4] and [(*R*)-**5f**][BF_4] presented mirror-image curves (blue and red), the presence of anionic counterion Δ-TRISPHAT provoked non-reciprocal spectra for [(*S*)-**5f**][Δ-**8**] (pink) and [(*R*)-**5f**][Δ-**8**] (light blue). In practice, a direct quantitative relationship between the intensity of the Cotton effects and the diastereoselectivity measured in NMR could not be found. Nevertheless, the presence of both stereogenic elements can increase the g_{abs} value up to 9 10^{-5} for most favored [(*R*)-**5f**][Δ-**8**]; g_{abs} curves being displayed in Fig. S4.

Conclusions

In summary, an acid-mediated skeletal rearrangement of cationic diaza[4]helicenes was developed to provide access to

unprecedented regioisomeric 1,11- and 3,11-DMQA scaffolds, not readily available by direct functionalization. This transformation, followed by aerobic photooxidation, converts parent 1,13-substituted system **1** into new cationic **2** and **3** [4]helicenes, thus complementing existing LSF methods. The rearranged cores can be further diversified by selective S_NAr processes or by regioselective demethylation/refunctionalization, giving a broad family of unsymmetrical dyes **4**–**7**. Structural changes have a clear impact on electronic and optical properties, with progressive blue shifts, improved fluorescence efficiencies in many cases, and small but definite substituent-dependent modulation across the visible range. X-ray and solution studies further show that peripheral editing of the helical framework reduces steric congestion in the cove region and strongly lowers the configurational barrier. As a result, the new helicenes are not configurationally stable but dynamically chiral, with enantiomerization barriers of around 19 kcal mol^{-1}. This feature makes them responsive to asymmetric environments, as shown by modest yet measurable inductions using chiral appendages and/or enantiopure TRISPHAT counterions. Overall, the present work demonstrates that skeletal rearrangement emerges as a powerful complement to late-stage functionalization for controlling the structure, photophysics, and chiral dynamics of cationic [4]helicenes.

Author contributions

Investigation: AG, RD, CH, CB (crystallography), GP (computation); funding acquisition and supervision: JL; writing – original draft: AG, CB, GP, JL; writing – review & editing: all.

Conflicts of interest

There are no conflicts to declare

Data availability

CCDC 2542615, 2542616, 2319499 and 2319500 contain the supplementary crystallographic data for this paper.[34a,b,c,d]

The data that support the findings of this study have been uploaded and will be openly available in yareta.unige.ch at https://doi.org/10.26037/yareta:dthr7jssmrcndfkvk6bjc7t4ta upon acceptance of the manuscript. It will be preserved for 10 years.

Supplementary information (SI) is available. See DOI: https://doi.org/10.1039/d6sc03190k.

Acknowledgements

We thank the University of Geneva and the Swiss National Science Foundation (200020-184843 and 200020-207539) for financial support. Open access funding was provided by the University de Geneva. Stéphane Grass (University of Geneva) for help in preparing synthetic materials. We thank Prof. Eric Vauthey and Dr Ricardo Fernández-Terán (University of Geneva) for giving access to the time-correlated single photon counting setup. G. P. acknowledges the University of Pisa for the availability of high-performance computing resources and support through the service computing@unipi.

Notes and references

1 (*a*) H. K. Singh, A. Bodzioch, A. Pietrzak and P. Kaszyński, *Chem. Commun.*, 2025, **61**, 496–499; (*b*) M. Qiu, J. Du, N.-T. Yao, X.-Y. Wang and H.-Y. Gong, *Beilstein J. Org. Chem.*, 2025, **21**, 1422–1453; (*c*) N. Hano, N. Zigon, B. Kuppan, L. Sturm, N. Vanthuyne, E. Pouget, S. Nlate, H. Bock, F. Durola, N. Avarvari and R. Oda, *Nanoscale*, 2025, **17**, 5081–5089; (*d*) Y. Gisbert, M. Ovalle, C. N. Stindt, R. Costil and B. L. Feringa, *Angew. Chem., Int. Ed.*, 2025, **64**, e202416097; (*e*) X. Xiao, Q. Cheng, S. T. Bao, Z. Jin, S. Sun, H. Jiang, M. L. Steigerwald and C. Nuckolls, *J. Am. Chem. Soc.*, 2022, **144**, 20214–20220; (*f*) B. Teichmann, A.-M. Krause, M.-J. Lin and F. Würthner, *Angew. Chem., Int. Ed.*, 2022, **61**, e202117625; (*g*) J. L. Rushworth, A. R. Thawani, E. Fajardo-Ruiz, J. C. M. Meiring, C. Heise, A. J. P. White, A. Akhmanova, J. R. Brandt, O. Thorn-Seshold and M. J. Fuchter, *JACS Au*, 2022, **2**, 2561–2570; (*h*) J. Crassous, I. G. Stará and I. Stary, *Helicenes: Synthesis, Properties, and Applications*, John Wiley & Sons, 2022; (*i*) T. Mori, *Chem. Rev.*, 2021, **121**, 2373–2412; (*j*) V. Hutskalova, A. Prescimone and C. Sparr, *Helv. Chim. Acta*, 2021, **104**, e2100182.

2 (*a*) I. G. Stará and I. Starý, in *Molecular Nanographenes*, 2025, pp. 105–148; (*b*) T. Edlova, J. Rybáček, H. Cattey, J. Vacek, L. Bednarova, P. Le Gendre, A. T. Normand, I. G. Stara and I. Starý, *Angew. Chem., Int. Ed.*, 2025, **64**, e202414698; (*c*) G. Zhang, J. Zhang, Y. Tao, F. Gan, G. Lin, J. Liang, C. Shen, Y. Zhang and H. Qiu, *Nat. Commun.*, 2024, **15**, 5469; (*d*) Z. Sun, W. Xu, S. Qiu, Z. Ma, C. Li, S. Zhang and H. Wang, *Chem. Sci.*, 2024, **15**, 1077–1087; (*e*) K. Mutoh and J. Abe, *Chem. Sci.*, 2024, **15**, 13343–13350; (*f*) P. Izquierdo-García, J. M. Fernández-García, S. Medina Rivero, M. Šámal, J. Rybáček, L. Bednárová, S. Ramírez-Barroso, F. J. Ramírez, R. Rodríguez, J. Perles, D. García-Fresnadillo, J. Crassous, J. Casado, I. G. Stará and N. Martín, *J. Am. Chem. Soc.*, 2023, **145**, 11599–11610; (*g*) Y. Wang, Z.-G. Wu and F. Shi, *Chem Catal.*, 2022, **2**, 3077–3111; (*h*) D. Reger, P. Haines, K. Y. Amsharov, J. A. Schmidt, T. Ullrich, S. Bönisch, F. Hampel, A. Görling, J. Nelson, K. E. Jelfs, D. M. Guldi and N. Jux, *Angew. Chem., Int. Ed.*, 2021, **60**, 18073–18081; (*i*) S. Huang, H. Wen, Y. Li, W. Qin, P. Wang, Y. Lan, S. Jia and H. Yan, *Nat. Commun.*, 2025, **16**, 500; (*j*) S. Herzog, G. G. Rizzo and J. Podlech, *Eur. J. Org Chem.*, 2024, **27**, e202301240; (*k*) S.-M. Guo, S. Huh, M. Coehlo, L. Shen, G. Pieters and O. Baudoin, *Nat. Chem.*, 2023, **15**, 872–880; (*l*) W. Fu, V. Pelliccioli, M. von Geyso, P. Redero, C. Böhmer, M. Simon, C. Golz and M. Alcarazo, *Adv. Mater.*, 2023, **35**, 2211279; (*m*) F. Fontana and B. Bertolotti, *Molecules*, 2022, **27**, 2522; (*n*) I. G. Stará and I. Starý, *Acc. Chem. Res.*, 2020, **53**, 144–158; (*o*) Y. Takeda, M. Okazaki, Y. Maruoka and S. Minakata, *Beilstein J. Org. Chem.*, 2015, **11**, 9–15; (*p*) T. J. Katz, L. Liu, N. D. Willmore,

J. M. Fox, A. L. Rheingold, S. Shi, C. Nuckolls and B. H. Rickman, *J. Am. Chem. Soc.*, 1997, **119**, 10054–10063.

3 (*a*) E. Tacke, L. Estaque, M.-D. Hoang, P. Durand, G. Clavier, G. Pieters and A. Chevalier, *Chem. Eur J.*, 2025, **31**, e202403684; (*b*) J. Stanojkovic, N. Terenti and M. C. Stuparu, *JACS Au*, 2025, **5**, 1707–1716; (*c*) K. Fujikata, M. Gon, K. Tanaka, Y. Chujo, A. Tsurusaki and K. Kamikawa, *Macromolecules*, 2023, **56**, 4550–4555; (*d*) K. Morioka, K. Wakamatsu, E. Tsurumaki and S. Toyota, *Chem. Eur J.*, 2022, **28**, e202103694; (*e*) T. Yanagi, T. Tanaka and H. Yorimitsu, *Chem. Sci.*, 2021, **12**, 2784–2793; (*f*) L. Guillemard, N. Kaplaneris, L. Ackermann and M. J. Johansson, *Nat. Rev. Chem.*, 2021, **5**, 522–545; (*g*) J. D. Jensen, N. Bisballe, L. Kacenauskaite, M. S. Thomsen, J. Chen, O. Hammerich and B. W. Laursen, *J. Org. Chem.*, 2021, **86**, 17002–17010; (*h*) J. Bosson, G. M. Labrador, C. Besnard, D. Jacquemin and J. Lacour, *Angew. Chem., Int. Ed.*, 2021, **60**, 8733–8738; (*i*) M. Jakubec and J. Storch, *J. Org. Chem.*, 2020, **85**, 13415–13428; (*j*) J. Börgel and T. Ritter, *Chem*, 2020, **6**, 1877–1887; (*k*) N. Yang, C. Shen, G. Zhang, F. Gan, Y. Ding, J. Crassous and H. Qiu, *Sci. Adv.*, 2023, **9**, eadg6680; (*l*) R. P. Kaiser, J. Ulč, I. Císařová and D. Nečas, *RSC Adv.*, 2018, **8**, 580–583; (*m*) J. W. Diesveld, J. H. Borkent and W. H. Laarhoven, *Recl. Trav. Chim. Pays-Bas*, 1980, **99**, 391–394.

4 (*a*) J. Bosson, N. Bisballe, B. W. Laursen and J. Lacour, in *Helicenes. Synthesis, Properties and Applications*, ed. J. Crassous, I. G. Stara and I. Stary, Wiley-VCH, 2022, ch. 4, pp. 127–165; (*b*) T. J. Sørensen, M. F. Nielsen and B. W. Laursen, *ChemPlusChem*, 2014, **79**, 1030–1035; (*c*) J. Bosson, J. Gouin and J. Lacour, *Chem. Soc. Rev.*, 2014, **43**, 2824–2840; (*d*) C. Herse, D. Bas, F. C. Krebs, T. Bürgi, J. Weber, T. Wesolowski, B. W. Laursen and J. Lacour, *Angew. Chem., Int. Ed.*, 2003, **42**, 3162–3166; (*e*) B. W. Laursen and F. C. Krebs, *Angew. Chem., Int. Ed.*, 2000, **39**, 3432–3434.

5 (*a*) I. H. Delgado, S. Pascal, A. Wallabregue, R. Duwald, C. Besnard, L. Guénée, C. Nançoz, E. Vauthey, R. C. Tovar, J. L. Lunkley, G. Muller and J. Lacour, *Chem. Sci.*, 2016, **7**, 4685–4693; (*b*) R. Duwald, S. Pascal, J. Bosson, S. Grass, C. Besnard, T. Bürgi and J. Lacour, *Chem. Eur J.*, 2017, **23**, 13596–13601; (*c*) Y. Nikolova, B. Fabri, P. Moneva Lorente, A. Guarnieri-Ibáñez, A. de Aguirre, Y. Soda, G. Pescitelli, F. Zinna, C. Besnard, L. Guénée, D. Moreau, L. Di Bari, E. Bakker, A. I. Poblador-Bahamonde and J. Lacour, *Angew. Chem., Int. Ed.*, 2022, **61**, e202210798; (*d*) J. Moutet, D. Mills, M. M. Hossain and T. L. Gianetti, *Mater. Adv.*, 2022, **3**, 216–223.

6 (*a*) B. Fabri, D. F. De Rosa, D. J. Black, R. Mucci, A. Krimovs, R. Pal and J. Lacour, *Chem. Eur J.*, 2025, **31**, e202501212; (*b*) B. Fabri, T. Funaioli, L. Frédéric, C. Elsner, E. Bordignon, F. Zinna, L. Di Bari, G. Pescitelli and J. Lacour, *J. Am. Chem. Soc.*, 2024, **146**, 8308–8319; (*c*) L. Frédéric, B. Fabri, L. Guénée, F. Zinna, L. Di Bari and J. Lacour, *Chem. Eur J.*, 2022, **28**, e202201853.

7 I. F. Yu, J. W. Wilson and J. F. Hartwig, *Chem. Rev.*, 2023, **123**, 11619–11663.

8 (*a*) R. H. Martin, J. Jespers and N. Defay, *Tetrahedron Lett.*, 1975, **16**, 1093–1096; (*b*) J. H. Borkent, P. H. F. M. Rouwette and W. H. Laarhoven, *Tetrahedron*, 1978, **34**, 2569–2571; (*c*) M. J. Fuchter, M. Weimar, X. Yang, D. K. Judge and A. J. P. White, *Tetrahedron Lett.*, 2012, **53**, 1108–1111; (*d*) R. J. F. Berger, M. J. Fuchter, I. Krossing, H. S. Rzepa, J. Schaefer and H. Scherer, *Chem. Commun.*, 2014, **50**, 5251–5253; (*e*) C. Matsuda, R. Igarashi, H. Katagiri and T. Murase, *Chem. Eur J.*, 2022, **28**, e202200132; (*f*) K. Seino, T. Okano, K. Oya, H. Katagiri and T. Murase, *Chem. Eur J.*, 2024, **30**, e202402445; (*g*) C. Shen, G. Zhang, Y. Ding, N. Yang, F. Gan, J. Crassous and H. Qiu, *Nat. Commun.*, 2021, **12**, 2786.

9 (*a*) J. Feng, L. Wang, X. Xue, Z. Chao, B. Hong and Z. Gu, *Org. Lett.*, 2021, **23**, 8056–8061; (*b*) M. Degač, L. Reininger, H. Schardax, E. Andris, L. Rulíšek, I. Císařová, U. Rinner, T. Cadart and M. Kotora, *JACS Au*, 2025, **5**, 4788–4798.

10 D. Hellwinkel, G. Aulmich and W. Warth, *Chem. Ber.*, 1980, **113**, 3275–3293.

11 (*a*) J. Guin, C. Besnard, P. Pattison and J. Lacour, *Chem. Sci.*, 2011, **2**, 425–428; (*b*) D. Conreaux, N. Mehanna, C. Herse and J. Lacour, *J. Org. Chem.*, 2011, **76**, 2716–2722; (*c*) B. Laleu, P. Mobian, C. Herse, B. W. Laursen, G. Hopfgartner, G. Bernardinelli and J. Lacour, *Angew. Chem., Int. Ed.*, 2005, **44**, 1879–1883.

12 J. P. Guthrie, *Can. J. Chem.*, 1978, **56**, 2342–2354.

13 Calculations on the three reduced compounds demonstrate the occurrence of large conformational ensembles for each moiety (Table S8). Overall, the calculations reveal strong relative stabilization of **2-H** and **3-H** with respect to **1-H** both in terms of internal and free energies. There is hence a clear thermodynamic driving force for the rearrangement from **1-H** to **2-H** and **3-H**.

14 A. Trummal, L. Lipping, I. Kaljurand, I. A. Koppel and I. Leito, *J. Phys. Chem. A*, 2016, **120**, 3663–3669.

15 With **1-Me** instead of **1-H**, the acidic mechanism generates tertiary *vs*. secondary cationic intermediates that are, at the same time, more stable but also more strained facilitating the rearrangement toward double MeO migration.

16 The oxidative C-C cleavage and the chemical nature of the "methyl" leaving group are of much scientific interest but a mechanistic study into this step was considered to be outside the scope of the current research. Further efforts are being pursued by the group.

17 (*a*) T. Yoshihara, H. Shudo, A. Yagi and K. Itami, *J. Am. Chem. Soc.*, 2023, **145**, 11754–11763; (*b*) J. Wang, P. Zhou and Y. Wang, *Eur. J. Org Chem.*, 2011, **2011**, 264–270; (*c*) P. V. Khodakovskiy, D. M. Volochnyuk, D. M. Panov, I. I. Pervak, E. V. Zarudnitskii, O. V. Shishkin, A. A. Yurchenko, A. Shivanyuk and A. A. Tolmachev, *Synthesis*, 2008, 948–956.

18 (*a*) A. M. Millimaci, R. V. Trilles, J. H. McNeely, L. E. Brown, A. B. Beeler and J. A. Porco, Jr., *J. Org. Chem.*, 2023, **88**, 13135–13141; (*b*) T. Iwata, R. Kawano, T. Fukami and M. Shindo, *Chem. Eur J.*, 2022, **28**, e202104160; (*c*) J. R. Frost, C. B. Cheong and T. J. Donohoe, *Synthesis*, 2017, **49**, 910–916; (*d*) J. R. Frost, C. B. Cheong, W. M. Akhtar,

D. F. J. Caputo, N. G. Stevenson and T. J. Donohoe, *J. Am. Chem. Soc.*, 2015, **137**, 15664–15667; (*e*) Y. Sun, P. Chen, D. Zhang, M. Baunach, C. Hertweck and A. Li, *Angew. Chem., Int. Ed.*, 2014, **53**, 9012–9016; (*f*) E. Macknight and R. A. McClelland, *Can. J. Chem.*, 1996, **74**, 2518–2527; (*g*) N. J. Hales, H. Heaney, J. H. Hollinshead and R. P. Sharma, *Tetrahedron*, 1995, **51**, 7403–7410.

19 S. G. Stenspil, A. H. Olsson, R. Mucci, M. Pink, C. Besnard, G. Pescitelli, J. Lacour, A. H. Flood and B. W. Laursen, *Angew. Chem. Int. Ed.*, 2024, e202412320.

20 J. Moutet, J. M. Veleta and T. L. Gianetti, *ACS Appl. Energy Mater.*, 2021, **4**, 9–14.

21 (*a*) O. Kel, P. Sherin, N. Mehanna, B. Laleu, J. Lacour and E. Vauthey, *Photochem. Photobiol. Sci.*, 2012, 623–631; (*b*) E. Pinosa, Y. Gelato, F. Calogero, M. M. Moscogiuri, A. Gualandi, A. Fermi, P. Ceroni and P. G. Cozzi, *Adv. Synth. Catal.*, 2024, **366**, 798–805; (*c*) K. A. Ryu, T. Reyes-Robles, T. P. Wyche, T. J. Bechtel, J. M. Bertoch, J. Zhuang, C. May, C. Scandore, N. Dephoure, S. Wilhelm, I. Quasem, A. Yau, S. Ingale, A. Szendrey, M. Duich, R. C. Oslund and O. O. Fadeyi, *ACS Catal.*, 2024, **14**, 3482–3491; (*d*) A. C. Shaikh, M. M. Hossain, J. Moutet, A. Kumar, B. Thompson, V. M. Huxter and T. L. Gianetti, *Angew. Chem., Int. Ed.*, 2025, **64**, e202420483; (*e*) N. Lal, Deepshikha, P. Singh and A. C. Shaikh, *Chem. Commun.*, 2025, **61**, 3005–3008; (*f*) M. M. Naiya, I. A. Guan, M. Sullivan, C. Eurtivong, E. Leung, L. I. Pilkington and D. Barker, *RSC Med. Chem.*, 2025, **16**, 2627–2640.

22 (*a*) M. Santella, E. Della Pia, J. K. Sørensen and B. W. Laursen, *Beilstein J. Org. Chem.*, 2019, **15**, 2133–2141; (*b*) T. J. Sørensen, D. Shi and B. W. Laursen, *Chem. Eur J.*, 2016, **22**, 7046–7049; (*c*) T. J. Sørensen and B. W. Laursen, *J. Org. Chem.*, 2010, **75**, 6182–6190; (*d*) J. B. Simonsen, K. Kjær, P. Howes, K. Nørgaard, T. Bjørnholm, N. Harrit and B. W. Laursen, *Langmuir*, 2009, **25**, 3584–3592; (*e*) C. Denekamp, J. Lacour, B. Laleu and E. Rabkin, *J. Mass Spectrom.*, 2008, **43**, 623–627; (*f*) B. W. Laursen, J. Reynisson, K. V. Mikkelsen, K. Bechgaard and N. Harrit, *Photochem. Photobiol. Sci.*, 2005, **4**, 568–576; (*g*) B. W. Laursen, F. C. Krebs, M. F. Nielsen, K. Bechgaard, J. B. Christensen and N. Harrit, *J. Am. Chem. Soc.*, 1998, **120**, 12255–12263.

23 (*a*) C. F. de Graauw, J. A. Peters, H. van Bekkum and J. Huskens, *Synthesis*, 1994, **1994**, 1007–1017; (*b*) J. S. Cha, *Org. Process Res. Dev.*, 2006, **10**, 1032–1053; (*c*) Y. Lu, F. Qu, B. Moore, D. Endicott and W. Kuester, *J. Org. Chem.*, 2008, **73**, 4763–4770; (*d*) Y. Lu, J. Bradshaw, Y. Zhao, W. Kuester and D. Kabotso, *J. Phys. Org. Chem.*, 2011, **24**, 1172–1178; (*e*) M. Sai, *Adv. Synth. Catal.*, 2018, **360**, 3482–3487.

24 The tandem photoactivated oxidation of the alcohols and reduction of cations **2** or **4** is deemed less likely with these cations that are quite more electron-rich than the acridinium precursors. See C. Nicolas, C. Herse and J. Lacour, *Tetrahedron Lett.*, 2005, **46**, 4605–4608.

25 With isopropanol as solvent, TLC monitoring indicates a full reduction of **4b** into **4b-H**. Oxidation of **4b-H** into **4b** occurs readily as ^{1}H-NMR analysis of an aliquot dissolved in $CDCl_3$ already shows a 50% conversion. Aerobic manipulations under regular laboratory light conditions are hence already sufficient for the reoxidation.

26 (*a*) M. Vogel, W. Rettig, R. Sens and K. H. Drexhage, *Chem. Phys. Lett.*, 1988, **147**, 452–460; (*b*) J. B. Grimm, B. P. English, J. Chen, J. P. Slaughter, Z. Zhang, A. Revyakin, R. Patel, J. J. Macklin, D. Normanno, R. H. Singer, T. Lionnet and L. D. Lavis, *Nat. Methods*, 2015, **12**, 244–250; (*c*) D. E. Nánási, M. B. Johansen, K. V. Mikkelsen and B. W. Laursen, *J. Am. Chem. Soc.*, 2026, **148**, 16290–16298.

27 M. H. Nowack and B. W. Laursen, *ChemPhotoChem*, 2025, **9**, e202500183.

28 J. S. S. K. Formen, J. R. Howard, E. V. Anslyn and C. Wolf, *Angew. Chem., Int. Ed.*, 2024, **63**, e202400767.

29 (*a*) J. Lacour, J. J. Jodry, C. Ginglinger and S. Torche-Haldimann, *Angew Chem. Int. Ed. Engl.*, 1998, **37**, 2379–2380; (*b*) S. Zahn and J. W. Canary, *Science*, 2000, **288**, 1404–1407; (*c*) V. Desvergnes-Breuil, V. Hebbe, C. Dietrich-Buchecker, J.-P. Sauvage and J. Lacour, *Inorg. Chem.*, 2003, **42**, 255–257; (*d*) J.-P. Mazaleyrat, K. Wright, A. Gaucher, N. Toulemonde, M. Wakselman, S. Oancea, C. Peggion, F. Formaggio, V. Setnička, T. A. Keiderling and C. Toniolo, *J. Am. Chem. Soc.*, 2004, **126**, 12874–12879; (*e*) S. Tartaglia, D. Padula, P. Scafato, L. Chiummiento and C. Rosini, *J. Org. Chem.*, 2008, **73**, 4865–4873; (*f*) J. Ściebura, P. Skowronek and J. Gawronski, *Angew. Chem., Int. Ed.*, 2009, **48**, 7069–7072; (*g*) J. R. Howard, A. Bhakare, Z. Akhtar, C. Wolf and E. V. Anslyn, *J. Am. Chem. Soc.*, 2022, **144**, 17269–17276; (*h*) S. T. Bao, H. Jiang, C. Schaack, S. Louie, M. L. Steigerwald, C. Nuckolls and Z. Jin, *J. Am. Chem. Soc.*, 2022, **144**, 18772–18777; (*i*) D. Pál, C. Besnard, A. de Aguirre, A. I. Poblador-Bahamonde, G. Pescitelli and J. lacour, *Chem. Eur J.*, 2023, **29**, e202302169; (*j*) D. Pál and J. Lacour, *Dalton Trans.*, 2024, **53**, 2665–2669; (*k*) A. J. Rothenberger, I. Park, G. R. Kiel, D. A. Stanley and T. D. Tilley, *J. Am. Chem. Soc.*, 2025, **147**, 44733–44738; (*l*) M. Coehlo, L. Frédéric, L. Poulard, N. Ferdi, L. Estaque, A. Desmarchelier, G. Clavier, J.-P. Dognon, L. Favereau, M. Giorgi, J.-V. Naubron and G. Pieters, *Angew. Chem., Int. Ed.*, 2025, **64**, e202414490; (*m*) Y. Tanioka, R. Omasa, T. Okujima, H. Uno and M. Takase, *RSC Adv.*, 2026, **16**, 1988–1992.

30 C. A. Guido, F. Zinna and G. Pescitelli, *Chem. Rev.*, 2025, **125**, 10492–10656.

31 (*a*) J. Lacour, C. Ginglinger, C. Grivet and G. Bernardinelli, *Angew Chem. Int. Ed. Engl.*, 1997, **36**, 608–609; (*b*) F. Favarger, C. Goujon-Ginglinger, D. Monchaud and J. Lacour, *J. Org. Chem.*, 2004, **69**, 8521–8524.

32 J. Lacour and D. Moraleda, *Chem. Commun.*, 2009, 7073–7089.

33 (*a*) M. Reddy G.N., R. Ballesteros-Garrido, J. Lacour and S. Caldarelli, *Angew. Chem., Int. Ed.*, 2013, **52**, 3255–3258; (*b*) M. Oppermann, F. Zinna, J. Lacour and M. Chergui, *Nat. Chem.*, 2022, **14**, 739–745; (*c*) J. R. Rouxel, B. Rösner, D. Karpov, C. Bacellar, G. F. Mancini, F. Zinna, D. Kinschel, O. Cannelli, M. Oppermann, C. Svetina, A. Diaz, J. Lacour, C. David and M. Chergui, *Nat. Photonics*, 2022, **16**, 570–574.

34 (*a*) CCDC 2542615: Experimental Crystal Structure Determination, 2026, DOI: 10.5517/ccdc.csd.cc2rbsvr; (*b*) CCDC 2542616: Experimental Crystal Structure Determination, 2026, DOI: 10.5517/ccdc.csd.cc2rbsws; (*c*) CCDC 2319499: Experimental Crystal Structure Determination, 2026, DOI: 10.5517/ccdc.csd.cc2hvmkk; (*d*) CCDC 2319500: Experimental Crystal Structure Determination, 2026, DOI: 10.5517/ccdc.csd.cc2hvmll.